Title

The Molecular Basis for Binding of an Electron Transfer Protein to a Metal Oxide Surface

Journal

Journal of the American Chemical Society, 139(36)

ISSN

0002-7863

Authors

Fukushima, Tatsuya

Gupta, Sayan

Rad, Behzad

et al.

Publication Date

2017-09-13

DOI

10.1021/jacs.7b06560

Peer reviewed

JACS
JOURNAL OF THE AMERICAN CHEMICAL SOCIETY

Article

pubs.acs.org/JACS

The Molecular Basis for Binding of an Electron Transfer Protein to a Metal Oxide Surface

Tatsuya Fukushima,[†,§] Sayan Gupta,[§] Behzad Rad, Jose A. Cornejo, Christopher J. Petzold, Leanne Jade G. Chan, Rena A. Mizrahi,[‡] Corie Y. Ralston, and Caroline M. Ajo-Franklin*

Molecular Foundry, Molecular Biophysics and Integrated Biosciences, and Biological Systems and Engineering Divisions, Lawrence Berkeley National Laboratory, Berkeley, California 94720, United States

Supporting Information

ABSTRACT: Achieving fast electron transfer between a material and protein is a long-standing challenge confronting applications in bioelectronics, bioelectrocatalysis, and optobioelectronics. Interestingly, naturally occurring extracellular electron transfer proteins bind to and reduce metal oxides fast enough to enable cell growth, and thus could offer insight into solving this coupling problem. While structures of several extracellular electron transfer proteins are known, an understanding of how these proteins bind to their metal oxide substrates has remained elusive because this abiotic−biotic interface is inaccessible to traditional structural methods. Here, we use advanced footprinting techniques to investigate binding between the *Shewanella oneidensis* MR-1 extracellular electron transfer protein MtrF and one of its substrates, α-Fe_2O_3 nanoparticles, at the molecular level. We find that MtrF binds α-Fe_2O_3 specifically, but not tightly. Nanoparticle binding does not induce significant conformational changes in MtrF, but instead protects specific residues on the face of MtrF likely to be involved in electron transfer. Surprisingly, these residues are separated in primary sequence, but cluster into a small 3D putative binding site. This binding site is located near a local pocket of positive charge that is complementary to the negatively charged α-Fe_2O_3 surface, and mutational analysis indicates that electrostatic interactions in this 3D pocket modulate MtrF−nanoparticle binding. Strikingly, these results show that binding of MtrF to α-Fe_2O_3 follows a strategy to connect proteins to materials that resembles the binding between donor−acceptor electron transfer proteins. Thus, by developing a new methodology to probe protein−nanoparticle binding at the molecular level, this work reveals one of nature's strategies for achieving fast, efficient electron transfer between proteins and materials.

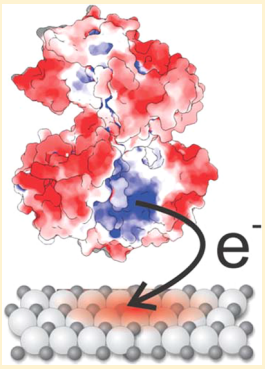

INTRODUCTION

Electron transfer between a protein and inorganic material forms the foundation for a wide range of enzyme- and microbe-based bioelectronic,[1] bioelectrocatalytic[2] and optobioelectronic[3] applications, including bioelectronic sensing,[1,4] solar production of fuels,[5] bioremediation,[6] biomining,[7] water purification,[8] and microbial[9] and enzymatic[10] fuel cells. The major scientific challenge in these fields is achieving electron transfer that is energetically efficient at a rate that is commensurate with enzyme turnover.[2,3,11] The coupling distance for direct electron transfer, which requires proper positioning of the redox site of the protein relative to the electrode material, varies between 10 and 30 Å.[12,13] To address this challenge, researchers have sought to orient enzymes on the electrode surface by displaying molecules on the electrode that mimic substrates of the enzyme,[14−19] by attaching molecules that penetrate the enzyme close to an electron relay center on the electrode,[20,21] and electrostatically directed covalent bonding of the protein to the electrode.[22] However, these approaches can only be applied to a limited set of enzymes and are frequently specific to an isozyme. Therefore, there exists a recognized need for new, generalizable strategies to enable oriented binding of proteins to materials to enable fast and efficient electron transfer.[2]

Interestingly, a class of naturally occurring proteins, extracellular electron transfer proteins, have the potential to inform a generalizable strategy for efficient protein-material electron transfer. Found primarily in metal-reducing microorganisms, these proteins transfer electrons derived from intracellular oxidative reactions to iron- or manganese-containing minerals as part of cellular respiration.[23] The most well-studied extracellular electron transfer proteins are MtrC, MtrF, and OmcA from *Shewanella oneidensis* MR-1, which reduce flavins, chelated Fe(III), Fe(II)oxides, and electrodes.[24] OmcA, MtrC, and MtrF, all extracellular surface-displayed decaheme cytochromes *c* (cyt *c*), adopt a similar three-dimensional fold composed of four domains which arrange 10 hemes in a staggered cross.[25−27] MtrC and MtrF are the terminal electron acceptors in the MtrCAB and MtrDEF porin-cyt *c* complexes which shuttle electrons across the outer membrane to the extracellular surface.[28] Recent quantum mechanical and molecular dynamics simulations of MtrF show that each heme has a different redox potential,[29−31] indicating that this enzyme regulates electron flux through the hemes. Under anaerobic conditions, MtrC and MtrF are most

Received: June 23, 2017
Published: August 14, 2017

DOI: 10.1021/jacs.7b06560
J. Am. Chem. Soc. 2017, 139, 12647−12654

important for reduction of extracellular Fe(III) oxides[32] and electrodes,[33] while OmcA appears to be somewhat less efficient in reducing these electron acceptors.[32]

A variety of biophysical measurements have sought to establish how OmcA, MtrC, and MtrF bind to minerals to accomplish electron transfer. These studies have established that OmcA and MtrC form bonds with the α-Fe_2O_3 surface[34] and that binding of OmcA to different surfaces induces conformational changes.[35−37] However, unlike other mineral-binding proteins,[38,39] OmcA, MtrC, and MtrF do not have repetitive stretches of residues in primary sequence that suggest a mineral binding site. On the basis of similarity to a hematite-binding peptide, it has been suggested that the Fe_2O_3 binding site in OmcA and MtrC is composed of a Ser/Thr-Pro-Ser/Thr sequence near heme 10.[40] However, a similar site is absent in MtrF, and molecular dynamics simulations of a model multiheme cyt *c*, Stc, with the α-Fe_2O_3 surface suggest a very different mode of binding, which is driven by hydrogen-bonding of heme propionates and acidic amino acids to the surface.[41] Thus, there is no consensus on what regions and interactions drive binding of these extracellular electron transfer proteins to their mineral substrates.[42]

Because MtrF efficiently catalyzes electron transfer to extracellular solids and its redox properties have been calculated,[29−31] we chose to use it as a prototype for studying the structural basis behind molecular recognition of metal oxides by extracellular electron transfer proteins. We examined the binding of MtrF to α-Fe_2O_3 nanoparticles using equilibrium binding measurements, protease footprinting, X-ray foot-printing mass spectrometry (XFMS), and site-directed muta-genesis. Surprisingly, we find that MtrF binds α-Fe_2O_3 specifically, but not tightly, and that this binding is mediated by complementary electrostatic interactions and induces few conformational changes in MtrF. Thus, using XFMS to probe solvent accessibility[43,44] in combination with other biophysical techniques shows that binding between MtrF and α-Fe_2O_3 resembles how electron transfer proteins recognize and bind to each other.

EXPERIMENTAL SECTION

Overexpression and Purification of MtrF and MtrF Variants. All primers, plasmids, and strains used in this study are shown in Tables S3 and S4 and detailed descriptions of the plasmid and strain construction are in the Supporting Information. In brief, to generate a version of MtrF that lacked a lipid anchor, we replaced the DNA sequence coding for the first 24 residues of MtrF with the coding sequence for first 24 residues of MtrB[26] to create plasmid I5077. Plasmids coding for additional MtrF mutants were prepared via site-directed mutagenesis using I5077 as the template. These plasmids were transformed into *E. coli* WM3064 and conjugated into *S. oneidensis* MR-1 to generate strains. The strains were used for MtrF overexpression. Overexpression and purification of the MtrF variants were performed as described previously[25] with slight variations (see Supporting Information).

Monitoring Binding between MtrF and Nanoparticles. We measured size of α-Fe_2O_3 nanoparticles using STEM imaging (see Supporting Information). Since the nanoparticles are irregularly shaped, we used the average surface area reported by the manufacturer, 147.5 m^2/g, for calculating the absorption constant (K_{ads}) and Gibbs free energy ($\Delta G^{\circ\prime}$). We monitored intrinsic tryptophan and tyrosine fluorescence to probe MtrF binding to α-Fe_2O_3 and α-Al_2O_3.[37,45] In brief, 3−6 mM α-Fe_2O_3 or 10 mM α-Al_2O_3 nanoparticles (Sigma-Aldrich, St. Louis, MO) were added to 100 nM MtrF and the resulting fluorescence from tyrosine and tryptophan residues was measured via fluorimetry (Jobin Yvon Fluoromax, HORIBA Scientific, Kyoto, Japan). The excitation and emission wavelengths were set to 280 nm and 305−380 nm, respectively, each with 5 nm slit widths. The changes in tryptophan fluorescence (360 nm) upon nanoparticle addition were identical to those in tyrosine fluorescence (310 nm) (data not shown). The FQ data was used for determining K_{ads} and $\Delta G^{\circ\prime}$ (see Supporting Information).

We also performed sedimentation assays to monitor MtrF binding to α-Fe_2O_3. In brief, 5 mM α-Fe_2O_3 was added to 0.5 μM MtrF and the mixture was incubated for 5 min at room temperature to permit binding. The mixture was centrifuged at 10 k rcf for 5 min, and then unbound MtrF in the supernatant was separated from MtrF bound to the nanoparticles in the pellet. The UV−visible spectrum of the supernatant was measured and the concentration of MtrF was determined using the Soret peak absorption at 410 nm. The sedimentation assay data was also used for determining K_{ads} (see Supporting Information).

Protease Footprinting Analysis. Samples composed of 2 μM MtrF in an appropriate buffer with and without 5 mM α-Fe_2O_3 nanoparticles were digested with 0.3 μg trypsin (Promega, Madison, WI) at pH 7 at 37 °C for 16 h, 0.3 μg chymotrypsin (Promega) at pH 7 at 37 °C for 16 h, or 0.3 μg pepsin (Sigma-Aldrich) at pH 4 at 37 °C for 6 h. After digestion, the samples were centrifuged at 10 k rcf for 5 min to pellet the nanoparticles, and the peptides in supernatant were subjected to LC−MS analysis. The peptides were analyzed using an Ascentis Peptides ES-C18 reverse phase column (2.1 mm × 100 mm, 2.7-μm particle size; Sigma-Aldrich) in an 1290 LC system coupled to 6550 iFunnel Q-TOF mass spectrometer (Agilent Technologies, San Jose, CA). Peptide mass identification and peptide MS/MS sequencing were carried out using Mascot (Matrix Science, Boston, MA) and MassHunter (Agilent Technologies) software. Additional details can be found in the Supporting Information.

XFMS Analysis. Samples composed of 1 μM MtrF with and without 2.5 mM nanoparticles were radiolyzed using 0, 300, 500, and 800 μs of X-ray exposure at beamline 5.3.1 as previously described.[44] To facilitate precise mass determination, the thioether bonds linking heme *c* to cysteine residues were cleaved and the free cysteines were carbamidomethylated after radiolysis. Additionally, to maximize the sequence coverage, we carried out three types of protease digestion with the exposed and carbamidomethylated MtrF samples. The resulting digested peptides were separated and identified by LC−MS methods as described in protease FP analysis. See the Supporting Information for additional experimental details.

RESULTS AND DISCUSSION

MtrF Binds Specifically to α-Fe_2O_3 Nanoparticles and Binds More Tightly at Lower pH. Native MtrF contains a lipoprotein signal sequence and must be solubilized using detergent during purification. To eliminate the need for detergent, which would complicate our experiments, we replaced the native lipoprotein signal sequence of MtrF with the signal sequence of MtrB[26] and expressed this construct in *S. oneidensis* MR-1. The MtrF protein was secreted into the culture medium, which facilitated subsequent purification. After purification, we confirmed the nonlipidated MtrF was soluble in the absence of detergent (Figure S1A), >90% pure (Figure S1B), full-length (Figure S1B,C), redox-active (Figure S1D), and contained 10 hemes (Figure S1F).

To examine the interactions of MtrF with Fe(III)oxides, we probed the binding of MtrF to 27 nm-diameter α-Fe_2O_3 nanoparticles (Figure S2A,B) using fluorescence quenching (FQ). Using nanoparticles of α-Fe_2O_3 afforded enough surface area to get good signal-to-noise in our FQ measurements. We observed that the fluorescence of MtrF was quenched relative to the initial fluorescence by addition of the α-Fe_2O_3 nanoparticles by as much as 80% (Figure 1A). To test if this binding was specific for α-Fe_2O_3 rather than minerals with the α-corundum lattice, we also probed FQ of MtrF with addition

DOI: 10.1021/jacs.7b06560
J. Am. Chem. Soc. 2017, 139, 12647−12654

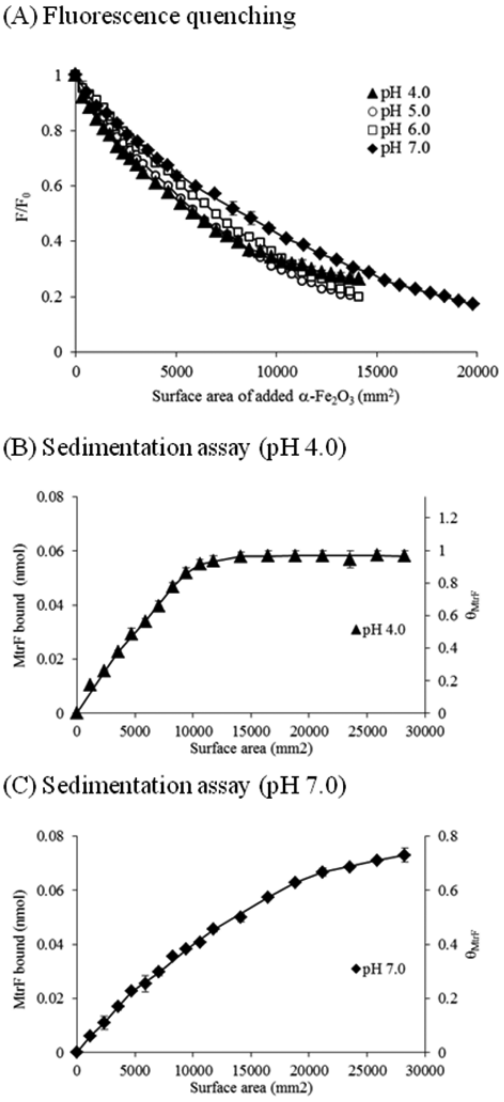

Figure 1. MtrF binds to α-Fe_2O_3 nanoparticles. (A) Fluorescence intensity relative to initial fluorescence intensity, F/F_o, of MtrF as a function of the surface area of added α-Fe_2O_3 nanoparticles at pH 4.0 (closed triangles), pH 5.0 (open circles), pH 6.0 (open squares) and pH 7.0 (closed diamonds). (B,C) Sedimentation assay of MtrF for the nanoparticles at pH 4.0 (B) and pH 7.0 (C). Data shows the average of two independent experiments and bars indicate the standard deviations. The calculated adsorption constants (K_{ads}) are shown in Table 1.

of α-Al_2O_3 nanoparticles. Fluorescence quenching was not observed by MtrF with the addition of the α-Al_2O_3 nanoparticles (Figure S2C), indicating that MtrF exhibits chemical specificity for binding to metal oxide surfaces. This chemical specificity likely reflects the difference in the surface structure of these metal oxides: the α-Fe_2O_3 surface contains Fe(III) singly coordinated with oxygen atoms,[46] while the terminal α-Al_2O_3 surface is covered by oxygen doubly coordinated to Al(III).[47]

Since the surface chemistry of α-Fe_2O_3 varies with pH, we hypothesized the binding of MtrF for the α-Fe_2O_3 nanoparticles might be affected by the pH. After determining that MtrF is stable between pH 4 and pH 8 (Figure S1E), we performed the FQ assay with MtrF in the range of pH 4−7. The binding of MtrF to α-Fe_2O_3 under weak acidic conditions was significantly tighter than the quenching at neutral pH (Figure 1A). The adsorption constants (K_{ads}) calculated using the FQ data show a 2-fold increase in the binding constant (K_{ads} at pH 4, 104 ± 3 × 10^{-6} mm^{-2}; K_{ads} at pH 7, 48 ± 2 × 10^{-6} mm^{-2}) (Table 1). To confirm these K_{ads}, we used a

Table 1. Calculated Adsorption Constants (K_{ads}) of MtrF

data used for the calculation	K_{ads}[a] (SD) × 10^{-6} [/mm^2]
FQ assay at pH 4.0	104(3)
FQ assay at pH 5.0	70(10)
FQ assay at pH 6.0	54(2)
FQ assay at pH 7.0	48(2)
Sedimentation assay at pH 4.0	138(2)
Sedimentation assay at pH 7.0	54(7)

[a]The adsorption constants (K_{ads}) were calculated using FQ and sedimentation data in Figure 1.

cosedimentation assay (Experimental Section). The binding constants of MtrF for the nanoparticles at pH 4 and pH 7 (Figure 1B,C, Table 1) were very similar to those measured by FQ, and again showed a 2-fold increase from pH 7 to pH 4. Thus, these data show that MtrF binds specifically to α-Fe_2O_3 nanoparticles and with a binding affinity that is ∼2-fold greater under weak acidic conditions compared to neutral conditions.

To put MtrF binding to α-Fe_2O_3 in the context of other extracellular electron transfer proteins and biomineralization proteins, we also analyzed the binding data using a Langmuir isotherm (see Supporting Information). We find that MtrF binds α-Fe_2O_3 nanoparticles at pH 7 with a standard Gibbs free energy ($\Delta G^{\circ\prime}$) of −55 kJ/mol. This is comparable in energy to the binding of OmcA to hematite, −28 kJ/mol,[37] but is ∼60 kJ/mol less favorable than the affinity of biomineralization proteins for their target minerals, e.g., binding of amelogenin for hydroxyapatite has $\Delta G^{\circ\prime}$∼ −120 kJ/mol.[48] These data indicate that MtrF and OmcA bind to minerals less tightly than typical biomineralization proteins.

Protease Footprinting Identifies a Region near Hemes 6 and 7 As a Possible Binding Site for α-Fe_2O_3 Nanoparticles. We next sought to determine what regions of MtrF bind most tightly to α-Fe_2O_3 nanoparticles. This abiotic−biotic interface is inaccessible to traditional structural techniques such as X-ray crystallography and NMR. Thus, we turned to protease footprinting, which probes accessibility of peptide bonds using proteolytic cleavage and has been used extensively to identify the interaction regions between proteins and their ligands.[49−51] Using multiple protease digestions, we probed solution accessibility of MtrF alone and the MtrF bound to α-Fe_2O_3 nanoparticles (MtrF:α-Fe_2O_3) at both pH 4 and pH 7. In the free protein, 154 proteolytic sites of MtrF, or 23% of its peptide bonds, were susceptible to digestion across these different experiments (Figure S3A). The identified proteolytic fragments covered 100% of the MtrF protein sequence (Figure S3A), showing protease footprinting effectively probes accessibility of MtrF.

The overall cleavage patterns from MtrF and MtrF:α-Fe_2O_3 were very similar, yet, a few very specific and significant differences stood out (Figure S3). No new proteolytic fragments were observed and no fragments became significantly more abundant upon α-Fe_2O_3 binding (Figure S3), strongly suggesting that binding did not trigger major conformational changes in MtrF. However, 10 proteolytic fragments, or ∼5% of the total, that appeared in the MtrF sample were undetectable in the α-Fe_2O_3:MtrF samples at pH 4 and pH 7 (Figure S3B). Analysis of this pattern indicates that the protease cleavage sites

DOI: 10.1021/jacs.7b06560
J. Am. Chem. Soc. 2017, 139, 12647−12654

at L460 and L515 are protected at pH 7 and sites L460, L469, F512, A608 and D609 are protected at pH 4 (Figure S3B). Protection of proteolytic sites upon ligand binding usually occurs near the binding site, suggesting that MtrF specifically binds α-Fe_2O_3 near these amino acids.

Mapping these six protected protease sites on the primary (Figure S4) and tertiary (Figure 2) structure of MtrF yields

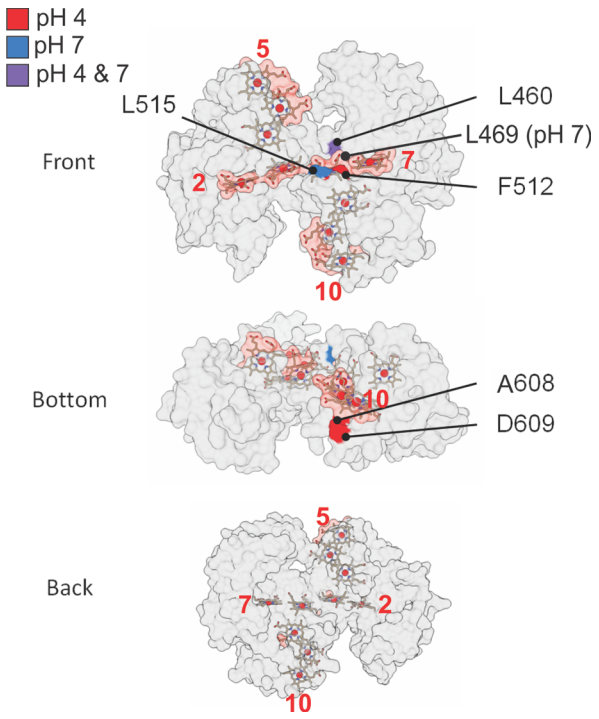

Figure 2. Protease footprinting shows that heme 6−7 region and heme 10 region of MtrF are protected by α-Fe_2O_3 nanoparticles. The solvent accessible regions of the protein and heme groups of MtrF (RCSB ID: 3PMQ) are shown as gray and light red surfaces, respectively, and are shown from different perspectives (front, bottom, back). Protease sites protected at pH 4, pH 7, and both pH 4 and 7 are indicated as red, blue and purple regions, respectively. The hemes are numbered in red according to their position in primary sequence. The detailed peptide maps of the protease FP are shown in Figure S3.

three striking observations. First, unlike binding sites in other material-binding proteins, these sites are not clustered in primary sequence, are not near regions of repetitive charge or hydrophobicity, and are not associated with any secondary structures (Figure S4). Second, there seem to be no sites of protection on the back side of the protein, i.e., the side of the MtrF lacking any exposed hemes (Figure 2), which is unlikely to be involved in electron transfer. Third, the six protected residues are clustered in a single domain (domain IV) in two regions within 0.7 nm of a heme cofactor: bounding a region of 150 $Å^2$ between hemes 6−7 (L460, L469, F512, L515) and 80 $Å^2$ near heme 10 (A608, D609) (Figure 2). Since electron transfer requires a heme to be within 1 nm of the mineral, these observations suggest that the regions between hemes 6 and 7 and heme 10 of MtrF bind to α-Fe_2O_3 to enable protein-mineral electron transfer.

XFMS Implicates an Area near Heme 6−7 as a Binding Site for α-Fe_2O_3 Nanoparticles. The protease footprinting qualitatively probes interactions that are sterically accessible to a large enzyme and stable on the hour time scale, which is much longer than the typical dissociation time found between relatively weak binders like MtrF and α-Fe_2O_3. Therefore, to determine the change in surface accessibility at higher resolution for the interactions between MtrF and α-Fe_2O_3, we turned to XFMS. In XFMS, a microsecond pulse of high-flux-density X-rays is used to generate reactive hydroxyl radicals in situ, and covalently modify solvent accessible side chains.[44,52] Since the rate of modification of an amino acid can be determined, XFMS reveals quantitative and ratiometric information on solvent accessibility changes.[53,54] We performed XFMS on both MtrF and α-Fe_2O_3:MtrF samples at pH 4 and pH 7. In the MtrF-only samples, we identified 16 peptide fragments corresponding to 13 different amino acids that were modified (Tables S1, S2). These amino acids were distributed throughout the solvent accessible protein surface (Figure 3), consistent with known mechanisms of action for hydroxyl radical modification.[44]

The XFMS labeling efficiency was independent of amount of Fe_2O_3 and therefore the method provided direct comparison of residue specific solvent accessibilities between free and bound sample. Therefore, we used the XFMS data for MtrF and MtrF:α-Fe_2O_3 to calculate R, the ratio of hydroxyl reactivity rate in MtrF:α-Fe_2O_3 to the reactivity rate in MtrF only (Figure 3B,C). In our study, $R > 1.5$ and $R < 0.5$ indicates a significant protection and increase in solvent accessibility of modifiable residues upon α-Fe_2O_3 binding, respectively. Similar to the protease footprinting experiments, at both pHs most of the residues did not show any significant change in solution accessibility ($R \sim 1$, Figure 3B,C). Likewise, no residues showed an increase in solvent accessibility, i.e., $R < 0.5$, indicating no significant conformational changes occurred (Figure 3B,C). However, a few residues were moderately ($1.5 < R < 1.75$) or strongly ($R > 1.75$) protected (Figure 3B,C, Tables S1, S2). As was the case for protease footprinting, all the protected residues are located on the heme-exposed side of MtrF (Figure 3A). Remarkably, of all 13 modified residues, the residue closest to the heme 6−7 region, M492, was strongly protected at pH 7. M211, which is near the heme 6−7 region, was also strongly protected, while the slightly more distant W81 was moderately protected (Figure 3C). The identification of the same heme 6−7 area as a protected region through two complementary techniques probing at different spatial and temporal resolution indicates that this region is involved in binding α-Fe_2O_3 at pH 7.

At pH 4, the XFMS protection pattern of MtrF by α-Fe_2O_3 also largely followed the protease footprinting pattern. First, both the degree and spatial extent of protection were greater at pH 4 compared to pH 7 (Figure 3A). Second, the three modifiable residues surrounding the possible binding site closest heme 6−7, M492, H216/L217 and M211, were all strongly protected from modification by nanoparticle binding at pH 4 (Figure 3A, B and Table S2). Overall, these observations indicate that MtrF specifically binds to α-Fe_2O_3 through a region between hemes 6 and 7 at pH 4 and 7.

Electrostatic Complementarity between the Binding Regions of MtrF and α-Fe_2O_3 Nanoparticles Contribute to Binding. To understand what interactions drive binding between this region of MtrF and α-Fe_2O_3, we used the crystal structure of MtrF and parametrized hemes to calculate the electrostatic map of MtrF at pH 7. Strikingly, the electrostatic map of MtrF (Figure 4) reveals that the largest region of positive charge on MtrF lies between hemes 6−7. Since the surface of α-Fe_2O_3 nanoparticles is negatively charged at pH 7 (zeta potential = −20 mV[55]), we hypothesized that

DOI: 10.1021/jacs.7b06560
J. Am. Chem. Soc. 2017, 139, 12647−12654

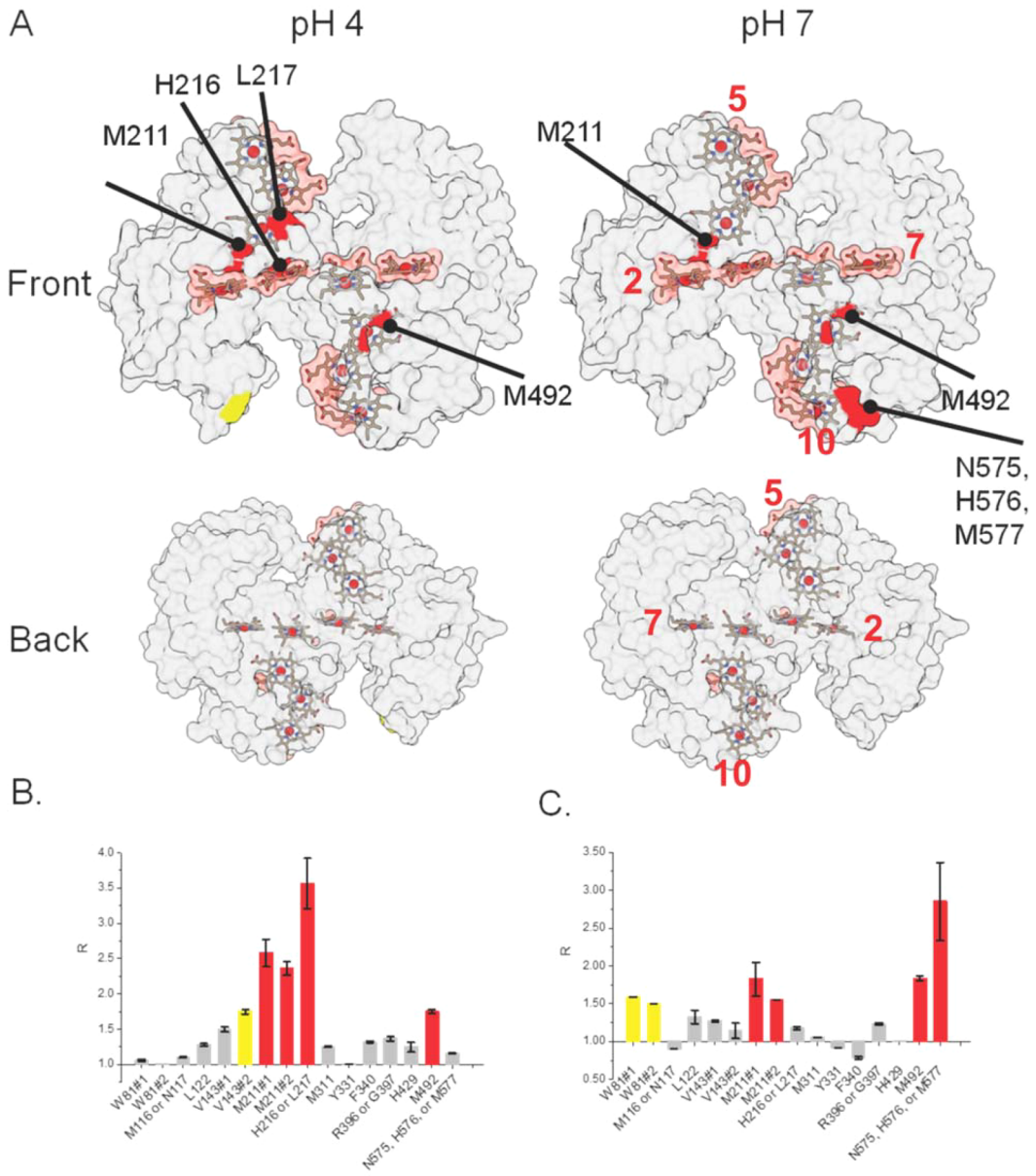

Figure 3. XFMS shows that amino acids located near heme 6−7 region and heme 10 of MtrF are protected by α-Fe_2O_3 nanoparticles. (A) Amino acid residues moderately (yellow) or strongly (red) protected by binding of the nanoparticles at pH 4 (left) and 7 (right) as viewed from the front and back perspective. The solvent accessible regions of the protein and heme groups of MtrF are shown as gray and light red surfaces, respectively. (B, C) Ratio of the modification rate for different amino acids in MtrF at pH 4 (B) and pH 7 (C). Gray bars indicate a modification rate ratio (MtrF alone /α-Fe_2O_3:MtrF) less than 1.5, whereas yellow residues indicate moderately protected residues (R = 1.5 to 1.7) and red residues are strongly protected residues (R > 1.7). The hemes are numbered in red according to their position in primary sequence.

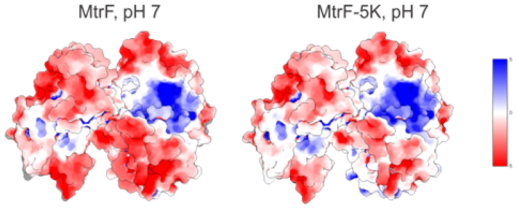

Figure 4. MtrF has a positively charged region which can be expanded by site-directed mutagenesis. (Left) Electrostatic map of MtrF at pH 7. (Right) Predicted electrostatic map of MtrF-5K mutant at pH 7.

complementary electrostatic interactions between the heme 6 and 7 region and the α-Fe_2O_3 surface mediate binding of MtrF to α-Fe_2O_3 nanoparticles.

To test this hypothesis, we mutated the protected residues from protease footprinting as single mutations and then in combination to an uncharged alanine, negatively charged aspartic acid, or positively charged lysine, and measured the binding of these purified MtrF mutants to α-Fe_2O_3 nanoparticles using FQ. The MtrF mutants containing only a single amino acid change at positions L460, F512, or L515 each bound α-Fe_2O_3 at pH 7 with similar affinity as wild-type MtrF (Table 2), regardless of the mutation. Changing these three amino acids simultaneously to alanine, L460A/F512A/L515A (MtrF-3A), did not significantly change the binding affinity of MtrF to α-Fe_2O_3. In contrast, the K_{ads} of the mutated MtrF with L460 K, F512 K, and L515 K (MtrF-3K) was significantly larger than the K_{ads} of the wild-type protein at pH 7 (Table 2,

DOI: 10.1021/jacs.7b06560
J. Am. Chem. Soc. 2017, 139, 12647−12654

Table 2. Calculated Adsorption Constants (K_{ads}) of MtrF Mutants

protein	K_{ads}[a] (SD) × 10^{-6} [/mm^2]	relative binding strength[b]
MtrF wild-type (pH 7)	52.0 (0.1)	1.00
MtrF wild-type (pH 4)	95 (4)	1.83
MtrF-L460A	53(2)	1.01
MtrF-L460D	61(4)	1.17
MtrF-L460K	59 (1)	1.13
MtrF-AA608−9	56(2)	1.09
MtrF-DD608−9	54(2)	1.03
MtrF-KK608−9	61(2)	1.18
MtrF-3A	52(6)	1.01
MtrF-3D	64 (0.4)	1.24
MtrF-3K	78(16)	1.50
MtrF-5K	98(4)	1.89

[a]The adsorption constants (K_{ads}) were calculated using FQ data in Figure 5 and S6. [b]Relative binding strength is calculated as K_{ads} of the mutants or MtrF wild-type (pH 4) divided by K_{ads} of the MtrF wild-type (pH 7).

Figure 5), showing that increasing positive charge near hemes 6 and 7 increases MtrF binding to the nanoparticles. Moreover,

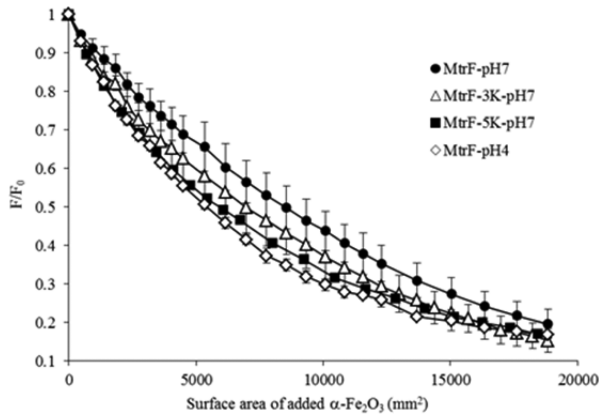

Figure 5. Mutations MtrF supports that amino acid residues protected by α-Fe_2O_3 nanoparticles from protease digestions are very important for binding of the nanoparticles. FQ assays of MtrF and its point-mutations for α-Fe_2O_3 nanoparticles at pH 7 and pH 4. MtrF-3K (open triangles), MtrF-5K (black squares) and the wild-type, MtrF at pH 7 (closed circles) and at pH 4 (open diamonds).

mutating MtrF to include positive charge near heme 10 (L460 K/F512 K/L515 K/A608 K/D609 K, MtrF-5K) further increases its binding to α-Fe_2O_3, such that its binding affinity is the same as wild-type MtrF's affinity to α-Fe_2O_3 at pH 4 (Table 2, Figure 5). This provides strong evidence that, at pH 7, electrostatic complementary between the positively charged region between hemes 6 and 7 and the negatively charged α-Fe_2O_3 surface modulates their binding.

New Strategies for Characterizing and Designing Protein-Material Binding. These results present new insight into the varying ways that mineral-binding proteins bind their solid substrates. In general, biomineralization proteins, which are frequently intrinsically disordered proteins,[56] use primary sequence regions to bind tightly to minerals ($\Delta G^{0\prime} \sim 120$ kJ/mol[48]) and undergo significant conformational changes[57] upon binding. Here we show MtrF uses complementary electrostatic interactions arising from tertiary structure to bind less tightly to its mineral substrate ($\Delta G^{0\prime} \sim 50$ kJ/mol) without undergoing significant conformational changes. Interestingly, these binding attributes more closely resemble the structural and energetic characteristics of electron transfer proteins in an electron transfer complex, which bind weakly (~25 kJ/mol)[58] using small intermolecular interaction surface area (>1000 Å^2) with few conformational changes.[59,60] While additional studies are needed to fill out the atomic details and kinetics of MtrF-α-Fe_2O_3 binding and their functional implications, it seems likely that the observed similarities to donor−acceptor protein−protein binding and dissimilarities to biomineralization protein arise from very different requirements for catalyzing electron transfer versus mineral growth. Most critically, our results illuminate that one strategy nature has used to yield efficient protein-material electron transfer is a relatively weak protein-material interaction, which involves few conformational changes and a small area of interfacial interaction.

Our results can also be used to understand better and engineer extracellular electron transfer in decaheme cyts *c*. The location of the MtrF binding site identifies hemes 6 and 7 as the likely donors for direct electron transfer to α-Fe_2O_3 at pH 7. Supporting this hypothesis, Breuer et al.[29,30] have shown via simulation that heme 7 in MtrF has the highest redox potential, making it the closest in redox potential to α-Fe_2O_3. Other decaheme cyts *c* also use regions near heme 7 to transfer electrons to different small molecule substrates, e.g., UndA with anthraquinone-2,6-disulfonate[61] or Fe_3OCit_3,[62] MtrC with flavin mononucleotide.[27] Thus, our work strengthens the idea that the heme 7 region plays a main role in transferring electrons to extracellular electron acceptors across different paralogs. This putative binding site also suggests that efforts to incorporate MtrF or other decaheme cyts *c* as a stand-alone[5,63,64] or microbially incorporated[1,65−67] bioelectrocatalysts should orient heme 7 to the electrode interface and suggests complementary electrostatic interactions are a means to direct this attachment.

Lastly, our results offer opportunities for characterization of protein-material interfaces for bioelectrocatalysis and optobioelectronic systems in their native protein environment. While researchers have directed enzyme attachment to electrodes using very strong covalent bonds[11,22] ($\Delta G^{0\prime} \sim 300$−400 kJ/mol), a more recent trend is to modify the electrode to mimic substrate-enzyme interactions, which are weaker ($\Delta G^{0\prime} \sim 25$−200 kJ/mol). In most cases, the strength of enzyme-electrode binding, the degree of binding-induced conformational changes in the protein, and the molecular-level protein−surface interactions are unknown or only known by computation.[68,69] Our work, in particular direct solvent accessibility measurements using XFMS in combination with other biophysical methods and mutational studies, presents a robust methodology for experimentally probing these key parameters in native conditions and for validating computational results.

CONCLUSIONS

To summarize, we found that MtrF binds specifically, but not tightly, to α-Fe_2O_3 nanoparticles. Remarkably, protease footprinting and XFMS indicate there are no significant conformational changes upon binding, but rather point to a very specific, small region in MtrF between hemes 6 and 7 as the nanoparticle binding site. Calculations and mutagenesis show that this binding is mediated by complementary electrostatic charges. These energetic and structural binding characteristics parallel binding between partner electron transfer. Thus, this

DOI: 10.1021/jacs.7b06560
J. Am. Chem. Soc. 2017, 139, 12647−12654

study of the interactions between MtrF and α-Fe_2O_3 nanoparticles establishes XFMS as a new way to characterize protein−material interactions at the molecular level and reveals one strategy nature has used to yield efficient protein-material electron transfer.

■ ASSOCIATED CONTENT

Supporting Information

The Supporting Information is available free of charge on the ACS Publications website at DOI: 10.1021/jacs.7b06560.

Additional experimental details and supporting protein characterization, footprinting, and XFMS data (PDF)

■ AUTHOR INFORMATION

Corresponding Author

*cajo-franklin@lbl.gov

ORCID

Caroline M. Ajo-Franklin: 0000-0001-8909-6712

Present Addresses

†Fornia BioSolutions, Inc., 3876 Bay Center Place, Hayward, California 94545, United States.

‡GigaGen, 407 Cabot Road, South San Francisco, California 94080, United States.

Author Contributions

§T.F. and S.G. contributed equally.

Notes

The authors declare no competing financial interest.

■ ACKNOWLEDGMENTS

We thank L. Shi for the gift of the LS plasmid, M. Charrier and B. Peng for preparing the point mutants, J. MacDonald and M. B. Francis for assistance with ESI-MS, R. Celestre and J. Feng for experimental support at beamline 5.3.1 of the ALS, and B. Cohen, M. A. TerAvest, J. A. Gralnick, R. Zuckermann and C. F. Blanford for helpful discussions. This work was supported by the Laboratory Directed Research and Development Program of Lawrence Berkeley National Laboratory, performed at the Molecular Foundry and the Advanced Light Source, and used resources of the Joint BioEnergy Institute, supported by the Office of Science, Office of Basic Energy Sciences and Office of Biological and Environmental Research, of the U.S. Department of Energy under Contract No. DE-AC02-05CH11231. CMA-F also acknowledges support from Office of Naval Research, Award number N000141310551.

■ REFERENCES

(1) TerAvest, M. A.; Ajo-Franklin, C. M. *Biotechnol. Bioeng.* **2016**, *113*, 687.

(2) Milton, R. D.; Wang, T.; Knoche, K. L.; Minteer, S. D. *Langmuir* **2016**, *32*, 2291.

(3) Wang, F.; Liu, X.; Willner, I. *Adv. Mater.* **2013**, *25*, 349.

(4) Bandodkar, A. J.; Wang, J. *Trends Biotechnol.* **2014**, *32*, 363.

(5) Ainsworth, E. V.; Lockwood, C. W.; White, G. F.; Hwang, E. T.; Sakai, T.; Gross, M. A.; Richardson, D. J.; Clarke, T. A.; Jeuken, L. J.; Reisner, E. *ChemBioChem* **2016**, *17*, 2324.

(6) Gadd, G. M. *Microbiology* **2010**, *156*, 609.

(7) Zhuang, W.-Q.; Fitts, J. P.; Ajo-Franklin, C. M.; Maes, S.; Alvarez-Cohen, L.; Hennebel, T. *Curr. Opin. Biotechnol.* **2015**, *33*, 327.

(8) Logan, B. E.; Elimelech, M. *Nature* **2012**, *488*, 313.

(9) Ieropoulos, I. A.; Greenman, J.; Melhuish, C.; Horsfield, I. *ChemSusChem* **2012**, *5*, 1020.

(10) Cosnier, S.; Gross, A. J.; Le Goff, A.; Holzinger, M. *J. Power Sources* **2016**, *325*, 252.

(11) Cracknell, J. A.; Vincent, K. A.; Armstrong, F. A. *Chem. Rev.* **2008**, *108*, 2439.

(12) Amdursky, N.; Marchak, D.; Sepunaru, L.; Pecht, I.; Sheves, M.; Cahen, D. *Adv. Mater.* **2014**, *26*, 7142.

(13) Gray, H. B.; Winkler, J. R. *Biochim. Biophys. Acta, Bioenerg.* **2010**, *1797*, 1563.

(14) Blanford, C. F.; Foster, C. E.; Heath, R. S.; Armstrong, F. A. *Faraday Discuss.* **2009**, *140*, 319.

(15) Cracknell, J. A.; McNamara, T. P.; Lowe, E. D.; Blanford, C. F. *Dalton Trans.* **2011**, *40*, 6668.

(16) Lalaoui, N.; Le Goff, A.; Holzinger, M.; Cosnier, S. *Chem. - Eur. J.* **2015**, *21*, 16868.

(17) Lalaoui, N.; Le Goff, A.; Holzinger, M.; Mermoux, M.; Cosnier, S. *Chem. - Eur. J.* **2015**, *21*, 3198.

(18) Lopez, R. J.; Babanova, S.; Ulyanova, Y.; Singhal, S.; Atanassov, P. *ChemElectroChem* **2014**, *1*, 241.

(19) So, K.; Kitazumi, Y.; Shirai, O.; Kano, K. *J. Electroanal. Chem.* **2016**, *783*, 316.

(20) Katz, E.; Sheeney-Haj-Ichia, L.; Willner, I. *Angew. Chem., Int. Ed.* **2004**, *43*, 3292.

(21) Xiao, Y.; Patolsky, F.; Katz, E.; Hainfeld, J. F.; Willner, I. *Science* **2003**, *299*, 1877.

(22) Rüdiger, O.; Abad, J. M.; Hatchikian, E. C.; Fernandez, V. M.; De Lacey, A. L. *J. Am. Chem. Soc.* **2005**, *127*, 16008.

(23) Weber, K. A.; Achenbach, L. A.; Coates, J. D. *Nat. Rev. Microbiol.* **2006**, *4*, 752.

(24) Shi, L.; Dong, H.; Reguera, G.; Beyenal, H.; Lu, A.; Liu, J.; Yu, H.-Q.; Fredrickson, J. K. *Nat. Rev. Microbiol.* **2016**, *14*, 651.

(25) Clarke, T. A.; Edwards, M. J.; Gates, A. J.; Hall, A.; White, G. F.; Bradley, J.; Reardon, C. L.; Shi, L.; Beliaev, A. S.; Marshall, M. J.; Wang, Z.; Watmough, N. J.; Fredrickson, J. K.; Zachara, J. M.; Butt, J. N.; Richardson, D. J. *Proc. Natl. Acad. Sci. U. S. A.* **2011**, *108*, 9384.

(26) Edwards, M. J.; Baiden, N. A.; Johs, A.; Tomanicek, S. J.; Liang, L.; Shi, L.; Fredrickson, J. K.; Zachara, J. M.; Gates, A. J.; Butt, J. N. *FEBS Lett.* **2014**, *588*, 1886.

(27) Edwards, M. J.; White, G. F.; Norman, M.; Tome-Fernandez, A.; Ainsworth, E. V.; Shi, L.; Fredrickson, J. K.; Zachara, J. M.; Butt, J. N.; Richardson, D. J.; Clarke, T. A. *Sci. Rep.* **2015**, *5*, 11677.

(28) White, G. F.; Shi, Z.; Shi, L.; Wang, Z.; Dohnalkova, A. C.; Marshall, M. J.; Fredrickson, J. K.; Zachara, J. M.; Butt, J. N.; Richardson, D. J.; Clarke, T. A. *Proc. Natl. Acad. Sci. U. S. A.* **2013**, *110*, 6346.

(29) Breuer, M.; Rosso, K. M.; Blumberger, J. *Proc. Natl. Acad. Sci. U. S. A.* **2014**, *111*, 611.

(30) Breuer, M.; Zarzycki, P.; Blumberger, J.; Rosso, K. M. *J. Am. Chem. Soc.* **2012**, *134*, 9868.

(31) Watanabe, H. C.; Yamashita, Y.; Ishikita, H. *Proc. Natl. Acad. Sci. U. S. A.* **2017**, *114*, 2916.

(32) Coursolle, D.; Gralnick, J. A. *Mol. Microbiol.* **2010**, DOI: 10.1111/j.1365-2958.2010.07266.x.

(33) Bücking, C.; Popp, F.; Kerzenmacher, S.; Gescher, J. *FEMS Microbiol. Lett.* **2010**, *306*, 144.

(34) Lower, B. H.; Shi, L.; Yongsunthon, R.; Droubay, T. C.; McCready, D. E.; Lower, S. K. *J. Bacteriol.* **2007**, *189*, 4944.

(35) Eggleston, C. M.; Vörös, J.; Shi, L.; Lower, B. H.; Droubay, T. C.; Colberg, P. J. *Inorg. Chim. Acta* **2008**, *361*, 769.

(36) Johs, A.; Shi, L.; Droubay, T.; Ankner, J. F.; Liang, L. *Biophys. J.* **2010**, *98*, 3035.

(37) Xiong, Y.; Shi, L.; Chen, B.; Mayer, M. U.; Lower, B. H.; Londer, Y.; Bose, S.; Hochella, M. F.; Fredrickson, J. K.; Squier, T. C. *J. Am. Chem. Soc.* **2006**, *128*, 13978.

(38) Evans, J. S. *Curr. Opin. Colloid Interface Sci.* **2003**, *8*, 48.

(39) Zheng, H.; Lu, Q.; Yan, B.; Huang, J.; Li, L.; Liao, Z. In *Bioadhesion and Biomimetics: From Nature to Applications*; Bianco-Peled, H., Davidovich-Pinhas, M., Eds.; CRC Press: Boca Raton, FL, 2015.

(40) Lower, B. H.; Lins, R. D.; Oestreicher, Z.; Straatsma, T. P.; Hochella, M. F., Jr; Shi, L.; Lower, S. K. *Environ. Sci. Technol.* **2008**, *42*, 3821.
(41) Kerisit, S.; Rosso, K. M.; Dupuis, M.; Valiev, M. *J. Phys. Chem. C* **2007**, *111*, 11363.
(42) Breuer, M.; Rosso, K. M.; Blumberger, J.; Butt, J. N. *J. R. Soc., Interface* **2015**, *12*, 20141117.
(43) Gupta, S.; Celestre, R.; Feng, J.; Ralston, C. *Synchrotron Radiation News* **2016**, *29*, 39.
(44) Gupta, S.; Celestre, R.; Petzold, C. J.; Chance, M. R.; Ralston, C. *J. Synchrotron Radiat.* **2014**, *21*, 690.
(45) Fukushima, T.; Sia, A. K.; Allred, B. E.; Nichiporuk, R.; Zhou, Z.; Andersen, U. N.; Raymond, K. N. *Proc. Natl. Acad. Sci. U. S. A.* **2012**, *109*, 16829.
(46) Trainor, T. P.; Chaka, A. M.; Eng, P. J.; Newville, M.; Waychunas, G. A.; Catalano, J. G.; Brown, G. E. *Surf. Sci.* **2004**, *573*, 204.
(47) Eng, P. J.; Trainor, T. P.; Brown, G. E., Jr; Waychunas, G. A.; Newville, M.; Sutton, S. R.; Rivers, M. L. *Science* **2000**, *288*, 1029.
(48) Friddle, R. W.; Battle, K.; Trubetskoy, V.; Tao, J.; Salter, E. A.; Moradian-Oldak, J.; De Yoreo, J. J.; Wierzbicki, A. *Angew. Chem., Int. Ed.* **2011**, *50*, 7541.
(49) Alonso, M. C.; van Damme, J.; Vandekerckhove, J.; Cross, R. A. *EMBO J.* **1998**, *17*, 945.
(50) Guan, J.-Q.; Chance, M. R. *Trends Biochem. Sci.* **2005**, *30*, 583.
(51) Underbakke, E. S.; Zhu, Y.; Kiessling, L. L. *J. Mol. Biol.* **2011**, *409*, 483.
(52) Xu, G.; Chance, M. R. *Chem. Rev.* **2007**, *107*, 3514.
(53) Chaudhuri, B. N.; Gupta, S.; Urban, V. S.; Chance, M. R.; D'Mello, R.; Smith, L.; Lyons, K.; Gee, J. *Biochemistry* **2010**, *50*, 1799.
(54) Gupta, S.; Guttman, M.; Leverenz, R. L.; Zhumadilova, K.; Pawlowski, E. G.; Petzold, C. J.; Lee, K. K.; Ralston, C. Y.; Kerfeld, C. A. *Proc. Natl. Acad. Sci. U. S. A.* **2015**, *112*, E5567.
(55) Pan, Z.; Somasundaran, P.; Turro, N.; Jockusch, S. *Colloids Surf., A* **2004**, *238*, 123.
(56) Oldfield, C. J.; Dunker, A. K. *Annu. Rev. Biochem.* **2014**, *83*, 553.
(57) Shaw, W. J. *Solid State Nucl. Magn. Reson.* **2015**, *70*, 1.
(58) Volkov, A. N.; Nicholls, P.; Worrall, J. A. *Biochim. Biophys. Acta, Bioenerg.* **2011**, *1807*, 1482.
(59) Lange, C.; Hunte, C. *Proc. Natl. Acad. Sci. U. S. A.* **2002**, *99*, 2800.
(60) Pelletier, H.; Kraut, J. *Science* **1992**, *258*, 1.
(61) Paquete, C. M.; Fonseca, B. M.; Cruz, D. R.; Pereira, T. M.; Pacheco, I.; Soares, C. M.; Louro, R. O. *Front. Microbiol.* **2014**, *5*, 318.
(62) Edwards, M. J.; Hall, A.; Shi, L.; Fredrickson, J. K.; Zachara, J. M. *Structure* **2012**, *20*, 1275.
(63) Lee, C.-Y.; Reuillard, B.; Sokol, K. P.; Laftsoglou, T.; Lockwood, C. W.; Rowe, S. F.; Hwang, E. T.; Fontecilla-Camps, J. C.; Jeuken, L. J.; Butt, J. N. *Chem. Commun.* **2016**, *52*, 7390.
(64) Reuillard, B.; Ly, K. H.; Hildebrandt, P.; Jeuken, L. J.; Butt, J. N.; Reisner, E. *J. Am. Chem. Soc.* **2017**, *139*, 3324.
(65) Jensen, H. M.; Albers, A. E.; Malley, K. R.; Londer, Y. Y.; Cohen, B. E.; Helms, B. A.; Weigele, P.; Groves, J. T.; Ajo-Franklin, C. M. *Proc. Natl. Acad. Sci. U. S. A.* **2010**, *107*, 19213.
(66) Sturm-Richter, K.; Golitsch, F.; Sturm, G.; Kipf, E.; Dittrich, A.; Beblawy, S.; Kerzenmacher, S.; Gescher, J. *Bioresour. Technol.* **2015**, *186*, 89.
(67) TerAvest, M. A.; Zajdel, T. J.; Ajo-Franklin, C. M. *ChemElectroChem* **2014**, *1*, 1874.
(68) Babanova, S.; Matanovic, I.; Chavez, M. S.; Atanassov, P. *J. Am. Chem. Soc.* **2015**, *137*, 7754.
(69) Matanovic, I.; Babanova, S.; Chavez, M. S.; Atanassov, P. *J. Phys. Chem. B* **2016**, *120*, 3634.

DOI: 10.1021/jacs.7b06560
J. Am. Chem. Soc. 2017, 139, 12647−12654